The International Journal of Advanced Manufacturing Technology (2018) 98:2865–2881
https://doi.org/10.1007/s00170-018-2415-x

ORIGINAL ARTICLE

# Modeling of cutting force, tool deflection, and surface error in micro-milling operation

Tesfaye M. Moges[1] · K. A. Desai[2] · P. V. M. Rao[1]

Received: 2 October 2017 / Accepted: 10 July 2018 / Published online: 26 July 2018


**Abstract**
Micro-milling has shown great potential in producing complex miniaturized components over wide range of materials. It can also fabricate micro-products in small batches efficiently and economically. In spite of these advantages, several challenges hinder its ability to produce components with better dimensional accuracy. Among several factors, tool deflection is one of the major sources of surface error on machined parts and features. Therefore, it is necessary to develop accurate and reliable process models to analyze and improve performance of the process. This study presents a methodology to determine cutting forces and surface error in the presence of tool deflections for micro-milling operation. Tool deflections have considerable influence on instantaneous uncut chip thickness. As tool deflection alters tooth trajectories and instantaneous uncut chip thickness, the rigid cutting force model needs to be modified suitably to consider the effect of deflections. This aspect has been incorporated in the model by modifying tool center location and tooth trajectories iteratively. The convergence of an iterative algorithm determining stable chip thickness is obtained by comparing RMS deviation of average chip thickness between two successive tooth passes. The axial variation of surface error due to tool deflections is estimated using surface generation mechanism. The proposed model is implemented in the form of a computational program to predict cutting force and surface error. The results of computational model are substantiated further by conducting machining experiments. It is shown that the proposed model predicts cutting forces fairly well in the presence of tool deflections. A comparison between predicted variation of surface error and 3D images of machined surface captured using optical microscope showed good qualitative agreement in the error profiles.

**Keywords** Micro-milling · Cutting force · Tool deflection · Uncut chip thickness · Surface error

## 1 Introduction

Micro-milling is one of the versatile processes used in aerospace, automobile, biomedical, and die-mold making industries to manufacture miniaturized components. It can produce complex 3-D micro- to meso-sized components and features in a wide range of materials with higher accuracy [1, 2]. Micro-milling is a down-scaled version of conventional milling, and both processes are apparently similar from operational point of view. Both variants remove work material mechanically in the form of chips by synchronized rotary and translatory motions between multi-teeth cutter and workpiece. The trochoidal trajectory formulation for cutting tooth is preferred in micro-milling in comparison to conventional milling where circular trajectory approximation is valid. This is primarily due to larger ratio of feed per tooth to tool radius in micro-milling. It has been demonstrated that the approximation as circular tooth trajectory results into significant error in modeling of micro-milling operation [3].

In spite of similarity from operational viewpoint, significant differences exist between both variants in terms of cutting phenomena and mechanics of chip formation due to size effect [4]. The edge radius of cutting tool is comparable to instantaneous uncut chip thickness in micro-milling as the edge is deliberately rounded to impart strength, prevent plastic

✉ K. A. Desai
kadesai@iitj.ac.in

Tesfaye M. Moges
tesfaye_mom@yahoo.com

P. V. M. Rao
pvmrao@mech.iitd.ac.in

[1] Department of Mechanical Engineering, Indian Institute of Technology Delhi, New Delhi 110016, India

[2] Department of Mechanical Engineering, Indian Institute of Technology Jodhpur, Jodhpur 342011, India

deformation, and avoid early tool breakage [5]. Therefore, chip formation occurs along the rounded edge of a tool resulting into negative value of effective rake angle though nominal rake angle is positive [6]. When chip thickness is less than the minimum limiting value, which depends on edge radius of a cutting tool and work material property, material removal does not occur in micro-milling. The cutting edge ploughs work material in this case instead of shearing and flows under the edge of cutting tool. The ploughed material gets elastically recovered and rubs flank face of the tool resulting into poor surface finish [7–9]. The subsequent cutting edge removes elastically recovered material withstanding higher chip load [10]. It has been shown that factors such as edge radius, minimum chip thickness, and elastic recovery of work material have significant effect on mechanics of chip formation [2, 9], cutting forces [7, 8, 11, 12], surface quality [13, 14], and burr formation [15]. It is also highlighted that the parameters such as spindle speed, feed rate, and built-up-edge have significant influence on the quality of micro-milled surface and burr formation [16, 17].

Tool deflection is another important factor limiting performance of micro-milling operation. A cutting tool used in micro-milling is prone to severe deflections due to significantly smaller value of diameter in comparison to overhang length. This results into drastic reduction of section modulus which lowers its strength and ability to withstand periodically varying cutting forces. The increased flexibility of cutting tool results into significant amount of deflections and thereby surface error on machined components. It has been shown in previous studies [18–20] that tool deflection is one of the major sources of surface error on parts made using micro-milling process. Therefore, it is important to model tool deflections and study its effect on mechanics of chip formation while predicting cutting forces and surface error. This paper presents a methodology to determine cutting force-induced tool deflections and develop a flexible force model considering effect of tool deflections on resultant cutting forces. The paper also presents a methodology to predict variation of machined surface error due to tool deflections. In the subsequent paragraphs, a comprehensive review of previous studies focusing on modeling of cutting forces, tool deflection and surface error in micro-milling is presented.

The prediction of tool deflection and surface error in micro-milling operation requires models determining process geometry and cutting forces along with mechanism to incorporate effects of tool deflection on the same. Past studies related to modeling of cutting forces in micro-milling can be broadly categorized into three groups: analytical, numerical and mechanistic models. Analytical models predict forces by correlating cutting forces with chip area through a set of analytical parameters determined on the basis of slip-line field theory [21–26]. The formulation used to calculate cutting force coefficients that correlate cutting forces and chip area requires prior knowledge of shear angle, mean friction angle, chip flow angle, tool-chip contact length and shear stress of work material. The precise determination of these parameters is difficult which limits application of the model. Numerical models predict cutting forces based on the principles of continuum mechanics by simulating real machining environment [27–29]. The model uses constitutive equations mainly Johnson-Cook model for different materials and Coulomb's friction model for coefficient of friction. The determination of parameters related to flow of work material, deformation rates, and friction coefficient are extremely difficult particularly at high temperature. A large number of assumptions are required in the model due to limitations of input in the computational software and large computational requirements, which limits application of the model. The mechanistic model relates cutting force components with chip area using cutting force coefficients. The effects of cutting parameters along with tool and work material properties are assumed to be integrated into coefficients without a priori analysis of mechanics of machining. The model is quite popular in literature as it does not require understanding of complex metal cutting mechanics and uses cutting coefficients which integrate the effect of cutting tool and work material properties. A review of previous studies conducted using mechanistic approach is only presented.

Li et al. [30] predicted cutting forces using mechanistic model considering effect of trochoidal trajectory, cutter runout, and minimum chip thickness. Perez et al. [31] estimated cutting forces using mechanistic model where cutting force coefficients were determined using experimental data. The cutting force coefficients were estimated as a function of uncut chip thickness using exponential relationship. Malekian et al. [32] developed mechanistic cutting force model for shearing and ploughing dominant regions considering minimum chip thickness and dynamics at the tool tip. The ploughing forces were estimated on the basis of interference volume between tool and workpiece considering the effect of elastic recovery. Jun et al. [33] proposed mechanistic force model considering effective rake and clearance angles and material pile-up in front of the cutting edge. Moges et al. [12] proposed a comprehensive mechanistic cutting force model incorporating process characteristics of micro-milling such as edge radius of cutting tool, minimum chip thickness, elastic recovery of work material, and change in effective rake and clearance angles. The above-mentioned research attempts have not considered the effect of tool deflection while predicting cutting forces. Tool deflection has significant effect on cutting forces as it changes uncut chip thickness which has direct relationship with cutting forces; therefore, it is important to incorporate its effects while predicting cutting forces in micro-milling operation. This requires prediction of tool deflections induced due to cutting action a priori in order to incorporate its effects on cutting forces.

Different approaches are presented in the literature to predict deflections of an end mill which can be broadly categorized into three groups. (a) Cantilever beam model with point force acting at a force center [34–36] which assumes application of point force at force center to predict deflections of end mill. (b) Cantilever beam model with non-uniform forces acting along cutter contact area. The model computes tool deflections by discretizing the end mill into finite disc elements along axial direction. The cutting forces computed from mechanistic force model can be directly applied to engaged axial disc elements and deflection of each node as well as total deflection can be computed [37, 38]. (c) FEA model which determines deflection of a cutting tool considering it as cantilever beam element e.g. Timoshenko beam element [39, 40].

Uriarte et al. [41] developed mechanistic force model for shearing and ploughing regions and used the same in predicting tool deflections. The tool deflection was computed by correlating resistance force due to deflections with forces acting on radial plane and static stiffness of tool measured at the tool tip. Rodríguez and Labarga [42] estimated tool deflections based on geometry of an end mill and theory of elasticity. In order to estimate deflection of end mill, distributed force along engaged portion of the flute is considered concentrated at a point and linear deflection profile is assumed. An important point to note here is that the chip thickness formulation of conventional milling is used to determine instantaneous chip thickness at micro-level which results into significant error as feed per tooth to tool radius ratio is relatively large in this case. Zhang et al. [43] developed mechanistic force model based on the work of Rodríguez and Labarga [42] considering trochoidal tooth trajectory and tool deflections. The study considered point force applied on the cutting tool instead of distributed force acting along engaged part of the tool which is not a realistic assumption. Mamedov et al. [44] predicted cutting force using mechanistic approach incorporating ploughing action based on interference volume between tool and workpiece. Tool deflection was computed by discretizing the cutter into finite elements in the axial direction and correlating cutting forces with stiffness matrix. Although the study considered two-dimensional Timoshenko beam element and used Cantilever beam model with non-uniform forces acting along cutter contact area to predicted tool deflection, the effect of tool deflection on cutting forces was not included in their predictive model. Wang et al. [45] proposed cutting force model considering minimum chip thickness, cutter runout, and tool deflection.

The past research attempts highlighted above determine deflection of a cutting tool in micro-milling, but limited effort has been made on incorporating its effects while predicting cutting forces and surface error. The existing models determine tool deflections assuming single point force acting on engaged part of the cutter which is not realistic and may result into inaccurate prediction. It is necessary to develop a realistic cutting force model incorporating effect of tool deflection along with important process characteristics of micro-milling such as edge radius of cutting tool, minimum chip thickness, elastic recovery of work material, and change in effective rake and clearance angles. Therefore, substantial improvement is required in the existing computational models to determine cutting forces and tool deflection-induced surface error in micro-milling.

The previous work of authors investigated the effect of cutter run-out on the process geometry parameters [10]. A set of process geometry parameters such as instantaneous uncut chip thickness and entry and exit angles of the flute is determined by considering run-out and elastic recovery of workpiece material. It is found that cutter run-out has substantial effect on these parameters in a wide range of feed per tooth values. The same methodology has been extended in the present work to incorporate tool deflection effects. This paper incorporates effect of tool deflections on cutting forces for developing flexible force model in micro-milling operation. This paper also proposes a methodology to predict tool deflection-induced surface error for components produced using micro-milling operation.

Henceforth, the paper is organized as follows: Section 2 presents summary of rigid force model adapted from previous study [12], tool deflection model proposed in the present study, an iterative algorithm to determine stable chip thickness, and flexible cutting forces along with surface generation mechanism. Section 3 presents comparison of predicted cutting forces with experimentally measured values. It also presents qualitative comparison of surface error predicted from the developed model with images of machined surface obtained from 3-D optical microscope. Section 4 summarizes the conclusions of the present work.

## 2 Modeling of cutting forces, tool deflections, and surface error

It has been highlighted in the previous section that an end mill is the most flexible element of micro-milling system and it deflects easily under the action of periodically varying cutting forces. Tool deflection in the normal direction causes significant error on machined surface which limits dimensional accuracy of the component and productivity of the process. Therefore, it is important to predict cutting forces and tool deflections accurately. It is also necessary to predict tool deflection-induced surface error as it helps in (a) obtaining desired dimensional tolerances, (b) devising compensation strategy, and (c) selecting of optimum cutting conditions. Firstly, the rigid cutting force model developed in previous research work [12] is summarized in this

section. The methodology to predict tool deflection is presented subsequently. Subsequently, an iterative algorithm is presented to determine stable chip thickness and flexible cutting force in the presence of tool deflection. Lastly, surface generation mechanism to predict tool deflection-induced surface error is presented. As tool deflection alters tooth trajectories and instantaneous uncut chip thickness, the cutting force model has to be modified suitably to consider the effect of deflections. An iterative scheme is presented to predict cutting forces in the presence of tool deflections.

## 2.1 Rigid cutting force model

A comprehensive mathematical model was developed by Moges et al. [12] incorporating important process characteristics of micro-milling process such as edge radius of the cutting tool, minimum chip thickness, elastic recovery of work material, and changes in the effective rake and clearance angles while predicting cutting forces. The study proposed portioning of cutting regions into two zones, namely, shearing dominant region (when chip thickness is greater than the minimum chip thickness ($h \geq h_{\min}$)) and ploughing dominant region (when chip thickness is less than the minimum chip thickness ($h < h_{\min}$)). The model predicts cutting forces by discretizing the process into steps; angle by angle, flute by flute, and the tool is segmented into disc elements along axial direction. The instantaneous uncut chip thickness has been determined by computing the shortest radial distance between current trajectory of a flute and previously generated surface considering cutter runout and elastic recovery of workpiece material [10], and the same is extended in the present study to incorporate the effect of tool deflection. Additionally, the model also divided uncut chip area, ploughed material, and elastically recovered work material along the flank side of the tool into finite number of elements to consider the change in rake and clearance angles effectively while determining normal and frictional forces.

The normal and frictional components of shearing force acting on an uncut chip element in shearing dominant region are determined using Eq. (1).

$$\left.\begin{aligned} dF_{\mathrm{fs}} &= K_{\mathrm{fs}} dA_{\mathrm{a}} \\ dF_{\mathrm{fs}} &= K_{\mathrm{fs}} dA_{\mathrm{a}} \end{aligned}\right\} \tag{1}$$

where $K_{\mathrm{ns}}$ and $K_{\mathrm{fs}}$ are cutting coefficients in shearing dominant region and $dA_{\mathrm{a}}$ is the area of an uncut chip element. The radial and tangential forces acting in a shearing dominant region are obtained as summation of shear forces acting on each chip element and edge forces which are expressed using Eq. (2) after performing coordinate transformations using effective rake angle ($\alpha_{\mathrm{e}}$).

$$\left.\begin{aligned} dF_{\mathrm{rs}} &= K_{\mathrm{re}} \frac{dz}{\cos\theta_{\mathrm{hx}}} + \sum_{u} \left[ \left( \Delta h_{\mathrm{s}} \cos\alpha_{\mathrm{e}} * \frac{dz}{\cos\theta_{\mathrm{hx}}} \right) \left( K_{\mathrm{ns}} \sin\alpha_{\mathrm{e}} + K_{\mathrm{fs}} \cos\alpha_{\mathrm{e}} \right) \right] \\ dF_{\mathrm{ts}} &= K_{\mathrm{te}} \frac{dz}{\cos\theta_{\mathrm{hx}}} + \sum_{u} \left[ \left( \Delta h_{\mathrm{s}} \cos\alpha_{\mathrm{e}} * \frac{dz}{\cos\theta_{\mathrm{hx}}} \right) \left( K_{\mathrm{ns}} \cos\alpha_{\mathrm{e}} - K_{\mathrm{fs}} \sin\alpha_{\mathrm{e}} \right) \right] \end{aligned}\right\} \tag{2}$$

Similarly, the normal and frictional components of ploughing forces acting on a given ploughed chip element and the normal and frictional components of the rubbing forces acting on an elastically recovered element are expressed using Eq. (3) and Eq. (4), respectively.

$$\left.\begin{aligned} dF_{\mathrm{np}} &= K_{\mathrm{np}} dA_{\mathrm{b}} \\ dF_{\mathrm{fp}} &= K_{\mathrm{fp}} dA_{\mathrm{b}} \end{aligned}\right\} \tag{3}$$

$$\left.\begin{aligned} dF_{\mathrm{nr}} &= K_{\mathrm{nr}} dA_{\mathrm{c}} \\ dF_{\mathrm{fr}} &= K_{\mathrm{fr}} dA_{\mathrm{c}} \end{aligned}\right\} \tag{4}$$

where $K_{\mathrm{np}}$ and $K_{\mathrm{fp}}$ are ploughing coefficients and $dA_{\mathrm{b}}$ is elemental ploughed area, and $K_{\mathrm{nr}}$ and $K_{\mathrm{fr}}$ are rubbing coefficients and $dA_{\mathrm{c}}$ is area of elastically recovered element. The radial and tangential forces acting in a ploughing dominant region are obtained by summing ploughing forces acting on each ploughed chip element, rubbing forces acting on each elastically recovered element, and the edge force acting on the cutting edge which are expressed using Eq. (5) after performing coordinate transformations using effective rake ($\alpha_{\mathrm{e}}$) and clearance ( $\gamma_{\mathrm{e}}$) angles.

$$\left.\begin{aligned} dF_{\mathrm{rp}} &= K_{\mathrm{re}} \frac{dz}{\cos\theta_{\mathrm{hx}}} + \sum_{v} \left[ \left( \Delta h_{\mathrm{p}} \cos\alpha_{\mathrm{e}} * \frac{dz}{\cos\theta_{\mathrm{hx}}} \right) \left( K_{\mathrm{np}} \sin\alpha_{\mathrm{e}} - K_{\mathrm{fp}} \cos\alpha_{\mathrm{e}} \right) \right] \\ &\quad + \sum_{w} \left[ \left( \Delta h_{\mathrm{er}} \cos\gamma_{\mathrm{e}} * \frac{dz}{\cos\theta_{\mathrm{hx}}} \right) \left( K_{\mathrm{nr}} \cos\gamma_{\mathrm{e}} + K_{\mathrm{fr}} \sin\gamma_{\mathrm{e}} \right) \right] \\ dF_{\mathrm{tp}} &= K_{\mathrm{te}} \frac{dz}{\cos\theta_{\mathrm{hx}}} + \sum_{v} \left[ \left( \Delta h_{\mathrm{p}} \cos\alpha_{\mathrm{e}} * \frac{dz}{\cos\theta_{\mathrm{hx}}} \right) \left( K_{\mathrm{np}} \cos\alpha_{\mathrm{e}} + K_{\mathrm{fp}} \sin\alpha_{\mathrm{e}} \right) \right] \\ &\quad + \sum_{w} \left[ \left( \Delta h_{\mathrm{er}} \cos\gamma_{\mathrm{e}} * \frac{dz}{\cos\theta_{\mathrm{hx}}} \right) \left( -K_{\mathrm{nr}} \sin\gamma_{\mathrm{e}} + K_{\mathrm{fr}} \cos\gamma_{\mathrm{e}} \right) \right] \end{aligned}\right\} \tag{5}$$

The cutting forces acting on a given axial disc element in Cartesian coordinate system are obtained by performing coordinate transformation of radial and tangential forces in ploughing and shearing dominant regions and can be expressed as Eq. (6).

$$\left.\begin{aligned} dF_x &= dF_r \sin\beta - dF_t \cos\beta \\ dF_y &= dF_r \cos\beta + dF_t \sin\beta \end{aligned}\right\} \tag{6}$$

where $\beta$ is instantaneous angular position of a cutting edge on a given axial disc element. The cutting forces determined in this manner are applied on engaged axial disc elements to

compute elemental tool deflection which has been discussed in the subsequent section.

## 2.2 Tool deflection model

A cutting tool is considered as a cantilever beam firmly supported in the tool holder at one end and subjected to non-uniform cutting forces acting along cutter contact area at the free end in this study. Due to action of cutting forces, tool deflects in feed (*X*-) and normal (*Y*-) directions of the cut while deflection along axial (*Z*-) direction is considered insignificant as it is absorbed by stiffness of the system. In order to predict deflections accurately, a tool has been divided into three separate geometric components: shank, taper and flute portion as each part has different geometric shape and configuration (Fig. 1a). The schematic representation of tool deflection model is shown in Fig. 1b. The concept of equivalent diameter of cutting tool has been used for the flute portion to consider the scaling effects [46].

The deflection of the fluted part is evaluated by considering non-uniformly distributed cutting forces acting on cutter contact area. This necessitates discretization of the fluted part into number of axial disc elements in the tool deflection model. As number of axial disc elements in the tool deflection and cutting force model are identical, the axial force values can be directly transferred to determine elemental tool deflections. For the shank and taper parts of the tool, point load acting at the tip of the end is considered and moment-area method is applied to compute the deflections. This assumption is considered reasonable as length of the tool from clamping position to the free end is quite larger compared to the axial depth of cut. The procedure to compute tool deflections in individual sections is given subsequently.

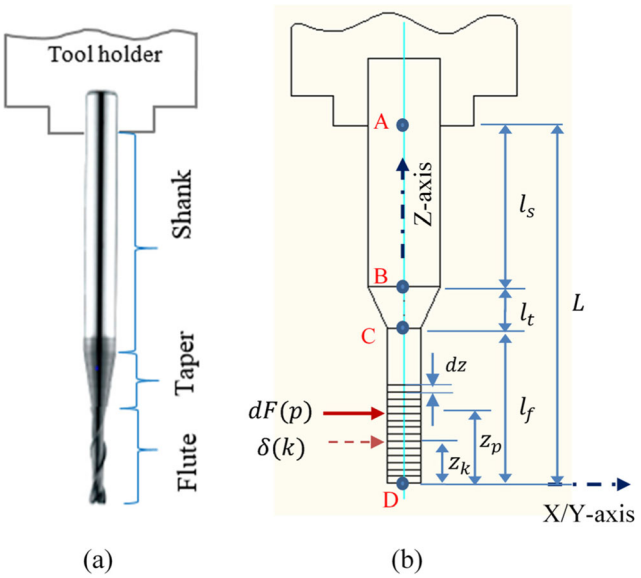


**Fig. 1** Tool deflection model of micro-end mill. (**a**) Parts of micro-end mill and (**b**) schematic representation

### 2.2.1 Deflection of the fluted part

The fluted part of the cutting tool is discretized into the same number of axial disc elements as cutting force model. Therefore, the magnitude of elemental force determined from the cutting force model can be directly applied to the cutter to determine elemental deflection values. Figure 2 shows the simplified free-body diagram of the fluted part with elemental load. The deflection equation has been derived from a cantilever beam model with elemental load acting on an engaged axial disc element.

Referring Fig. 1b and Fig. 2, the *X*- and *Y*- deflections of an individual axial disc element ($k$) due to force acting at $p$th disc element can be calculated using Eq. (7).

$$d\delta_{\mathrm{f}}(k,p) = \begin{Bmatrix} \frac{dFx^2}{6EI_f}(3a-x), & 0 < x < a \\ \frac{dFa^2}{6EI_f}(3x-a), & a < x < L_f \end{Bmatrix} \tag{7}$$

The total static deflection of each axial disc element can be computed using superposition of deflections produced by cutting forces applied on $m$ engaged axial disc element, and it can be expressed as Eq. (8).

$$\delta_{\mathrm{f}}(k) = \sum_{p=1}^{m} \delta_{\mathrm{f}}(k,p) \tag{8}$$

### 2.2.2 Deflection of taper and shank parts

The deflection of taper and shank parts of the cutter has been formulated using moment-area method assuming concentrated force applied at the free end of the tool at a given angle of rotation. The moment-area method is a semi-graphical method used to calculate deflection of the beam subjected to bending [47].

The deflection value at a particular location can be determined by multiplying area under *M*/*EI* diagram with the distance from the point of interest to the centroid of the area. The loading diagram (Fig. 3a), bending moment diagram (Fig. 3b), *M*/*EI* diagram (Fig. 3c), and deflection diagram (Fig. 3d) are shown in Fig. 3. The deflection of the tool at point *C* is expressed as summation of deflection of shank and taper parts.

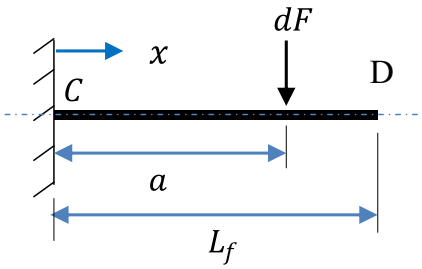


**Fig. 2** Free body diagram of fluted part

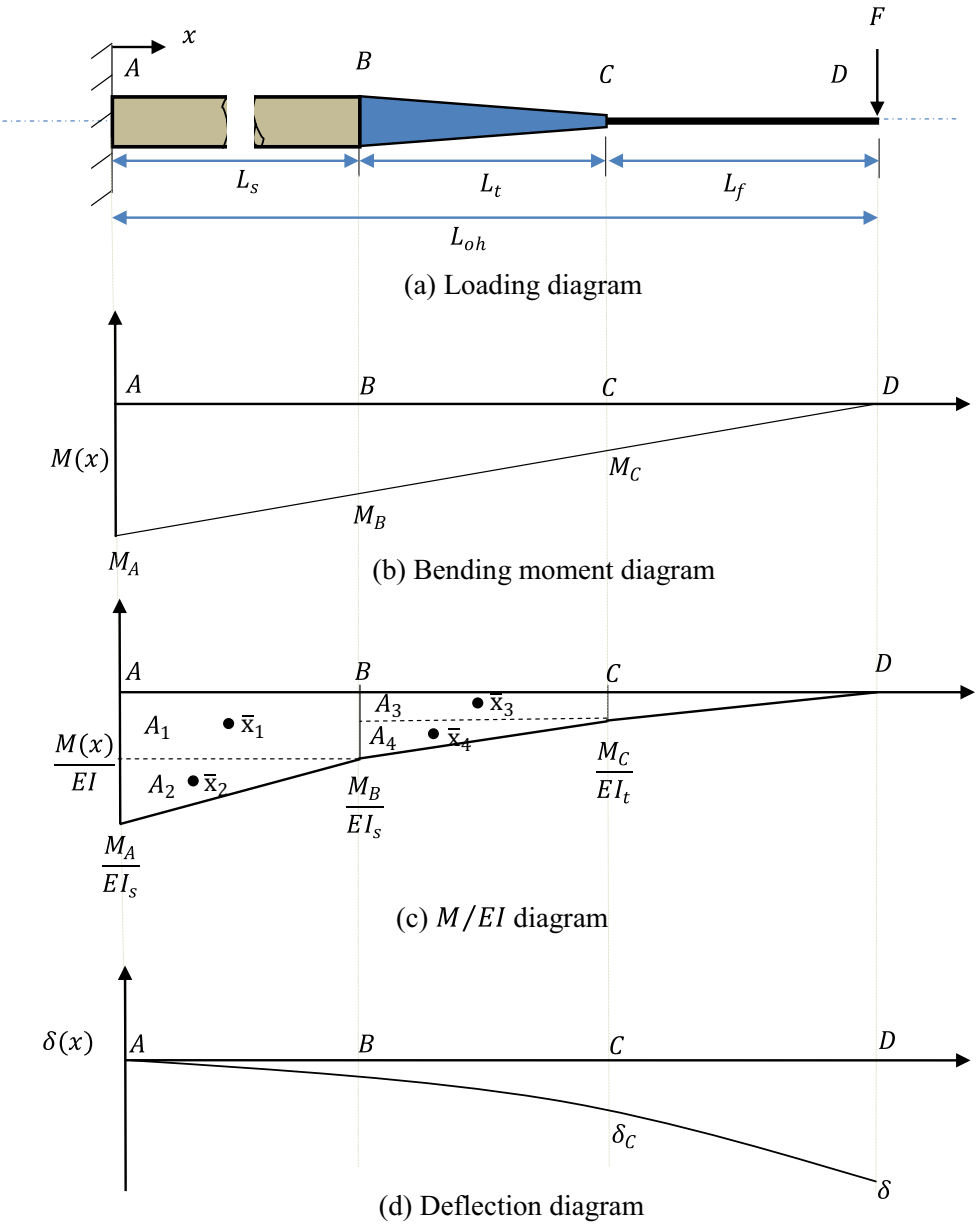


**Fig. 3** Calculation of deflection of shank and taper parts

In order to calculate deflection at point $C$, bending moments, areas under $M/EI$ diagram, and centroid locations of points $A$, $B$, and $C$ have been determined priorly. The expressions to determine these parameters are summarized in Table 1.

The deflection of shank and taper parts at point $C$ can be expressed using Eq. (9).

$$\delta_C = A_1 * \bar{x}_1 + A_2 * \bar{x}_2 + A_3 * \bar{x}_3 + A_4 * \bar{x}_4 \tag{9}$$

**Table 1** Expressions for bending moments, areas, and centroids of taper and shank parts

| Bending moment at points $A$, $B$, and $C$ | Expression | Area | Expression | Centroid location from point $C$ | Expression |
|---|---|---|---|---|---|
| $M_A$ | $F * L_{oh}$ | $A_1$ | $\frac{M_B}{EI_s} * L_s$ | $\bar{x}_1$ | $\frac{L_s}{2} + L_t$ |
| $M_B$ | $F * (L_{oh} - L_s)$ | $A_2$ | $\frac{1}{2} * \frac{1}{2} * L_s$ | $\bar{x}_2$ | $\frac{2L_s}{3} + L_t$ |
| $M_C$ | $F * (L_{oh} - (L_s - L_t))$ | $A_3$ | $\frac{M_C}{EI_t} * L_t$ | $\bar{x}_3$ | $\frac{L_t}{2}$ |
| | | $A_4$ | $\frac{1}{2} * \left(\frac{1}{2} - \frac{1}{2}\right) * L_t$ | $\bar{x}_4$ | $\frac{2L_t}{3}$ |

The deflection of axial disc element at a particular angle of rotation is expressed as summation of deflections at point $C$ determined using Eq. (9) and deflection of fluted part determined using Eq. (8). The total deflection can be determined using Eq. (10).

$$\delta(k) = \delta_C + \delta_f(k) \tag{10}$$

Based on deflection values computed in this manner, a new tool center along with revised tooth trajectories is to be determined and instantaneous uncut chip thickness has to be computed. The change of chip thickness results into modified cutting forces which are to be computed recursively. The subsequent section presents a methodology to predict such flexible cutting forces iteratively in the presence of tool deflections.

### 2.3 Flexible force model

In order to compute cutting forces realistically in the presence of tool deflections, it is required to incorporate the effect of deflections on determination of instantaneous uncut chip geometry. The change of chip geometry in conventional milling was highlighted by Sutherland and Devor [48] by proposing the concept of flexible force model which determines stable chip geometry iteratively and computes cutting forces. This concept has been extended to micro-milling operation in the present study. The estimated value of tool deflection determined in the previous section has been used to determine the new location of tool center and thereby tooth trajectories. The deflections of cutting tool cause position of tool center to deviate from the desired position as shown in Fig. 4. At a particular angular rotation, the tool center deviates from the nominal position $C_b(x_{Cb}, y_{Cb})$ to the deflected position $C_a(x_{Ca}, y_{Ca})$ by an amount equal to $\delta_x$ and $\delta_y$ in $X$- and $Y$-directions, respectively. The coordinates of tool center location $C_a(x_{ca}, y_{ca})$ after tool deflection can be determined using Eq. (11). The deflected coordinates of tool center has to be determined for each axial disc element.

$$\left.\begin{aligned} x_{Ca} &= x_{Cb} + \delta_x \\ y_{Ca} &= y_{Cb} + \delta_y \end{aligned}\right\} \tag{11}$$

The deflected coordinates of tool center determined using Eq. (11) differ from the desired center in both $X$- and $Y$- directions by an amount determined using tool deflection model outlined in the previous section. The chip geometry is to be computed subsequently using deflected tool center positions and tooth trajectories. The instantaneous uncut chip thickness is expressed as the shortest radial distance between the surface generated from previous tooth pass and trajectory of the current cutting edge at a given rotation angle. Figure 5 depicts geometrical computation of instantaneous uncut chip thickness in the presence of tool deflections. The trajectory of each tooth pass has been determined using process geometry model proposed by Moges et al. [10], and it is considered as the surface generated from the previous tooth pass to determine uncut chip thickness removed by current tooth pass. The coordinates of current tool center positions and corresponding tooth trajectory are determined considering deflection values determined in the previous section. The current tooth pass remains in the cut for shorter period and it exits early in the presence of tool deflections. Thus, the surface generated by current tooth pass is different from its trajectory. It can be seen from Fig. 5 that the surface generated by the current tooth is combination of surface generated from the previous tooth pass and current tooth trajectory which has been represented by thicker dashed curve in Fig. 5. It has been observed in earlier studies related to conventional milling that the difference between surface generated and tooth trajectory exists for the first few tooth passes only [49]. As a result, the chip load experienced by these tooth passes is not uniform and cutting forces vary significantly. The difference of chip load between tooth passes vanishes after few iterations and the process attains stable state. This results into identical surface generated by successive tooth passes and thereby removal of the same amount of material and cutting forces during each tooth pass.

An iterative scheme has been devised to determine such stable state of cutting in the computational models. It has been observed that the first tooth pass does not incorporate tool deflections in determining uncut geometry and cutting forces.

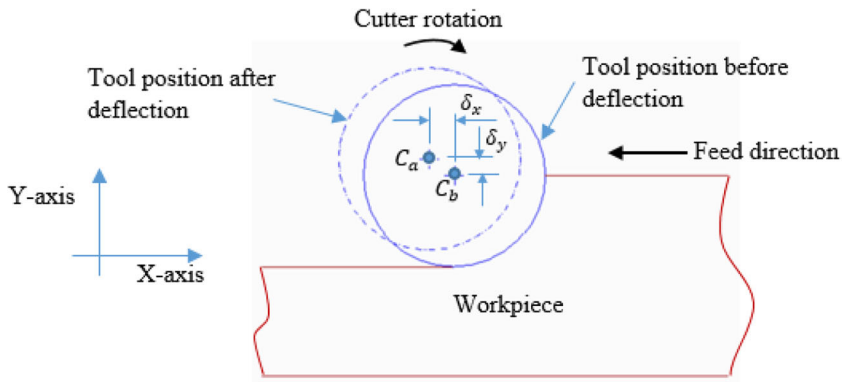


**Fig. 4** Deviation of tool center due to tool deflection

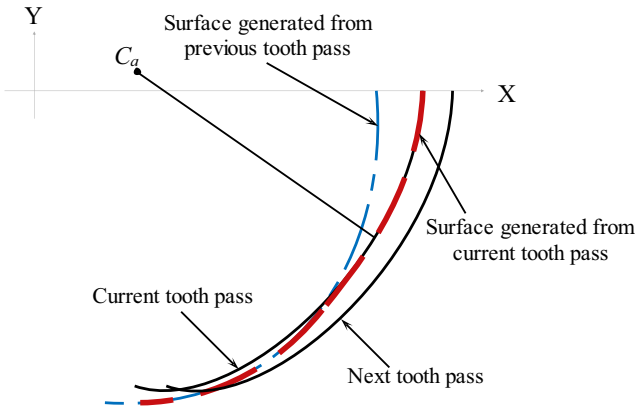


**Fig. 5** Determination of stable uncut chip thickness in the presence of tool deflections

The effect of tool deflection on center location and tooth trajectories has been incorporated in the model during second tooth pass. In order to examine the stable state of cutting and convergence, Root Mean Square (RMS) deviation is introduced in the computational algorithm. The algorithm determines instantaneous uncut chip thickness removed by each tooth pass as the shortest radial distance between the current tooth pass and surface generated by previous tooth pass at a given rotation angle. The RMS deviation is computed then as a difference of uncut chip thicknesses between these consecutive tooth passes which can be represented using Eq. (12). The convergence criterion $\varepsilon^* = 0.0005$ has been set in the algorithm to examine the stable state of cutting.

$$RMS\ error = \sqrt{\frac{\sum\left[(h_n(\theta) - h_{n-1}(\theta))^2\right]}{N}}, \qquad n = 2, 3, 4. \ . \ . \qquad (12)$$

where $h_n(\theta)$ and $h_{n-1}(\theta)$ are the uncut chip thickness to be removed by tooth pass $n$ and $n-1$ at each engaged angle of rotation ($\theta$). $N$ is the number of samples. $n$ is the number of tooth passes. Note that the uncut chip thickness for the first tooth pass has to be computed without considering tool deflection from rigid force model. This would be required to generate cutting force data for computation of deflections for the first time.

Once convergence is achieved, instantaneous uncut chip thickness removed by $n$th tooth pass is obtained as the shortest distance between the deflected trajectory of $n$th tooth pass and the surface generated by $(n-1)$th tooth pass. For each tooth pass, instantaneous uncut chip thickness is calculated considering tool deflections and RMS deviation is determined to achieve convergence of the algorithm. The cutting force, tool deflection and surface error values corresponding to each angular rotation are computed based on the stable chip thickness values. The overall computational algorithm to determine instantaneous uncut chip thickness, cutting forces, tool deflections, and surface error is depicted in Fig. 6. The entire computational scheme can be divided into three phases. The first phase predicts tool deflections for the first tooth pass using rigid cutting force and tool deflection models. The values of tool deflections computed during the first tooth pass has been used in computing deflected tool center positions and tooth trajectory which are used further in the second phase. The second phases of computational algorithm uses deflected center coordinates and tooth trajectories to compute stable chip thickness iteratively based on RMS deviation based convergence criterion. The third phase of the algorithm predicts flexible cutting forces considering tool flexibility in shearing and ploughing dominant regions based on uncut chip thickness computed using iterative algorithm. The surface error profile is then determined based on cutting forces obtained from the algorithm. The subsequent section presents a methodology to estimate variation of tool deflection-induced surface errors.

## 2.4 Modeling of surface error

Surface error in milling operation is determined as the deviation of machined surface from the desired one in the normal direction [34]. It has been highlighted by various researchers [18–20] that the deflection of cutting tool results into significant surface error on machined components (Fig. 7). It has been realized that a cutting tool may deflect either away (down-milling) or towards (up-milling) the workpiece producing either under or overcut, respectively. This implies that the machined surface is generated when cutting edge exits the cut in down milling while the same happens when an edge enters into the cut while up milling. The present study considers down milling mode of operation implying instantaneous angular position ($\beta$) for $i$th cutting edge on $k$th axial disc element as $\pi$ from $Y$- axis. The condition of surface generation in down milling can be expressed using Eq. (13). It has to be noticed here that the axial location of surface generation point varies with cutter rotation angle due to helix angle [50].

$$\beta(z) = \theta - (i)\varphi_p - \left(\frac{\tan\theta_{hx}}{\mathrm{r}}\right) z = \pi \qquad (13)$$

The surface generation methodology stores tool deflection in the normal direction at surface generation point as surface error. As $Y$- axis coincides with the normal direction, surface error $\varepsilon(k)$ at each axial disc element is equal to tool deflection $\delta_y(k)$ at a distance $z$ from the bottom of tool tip and it can be expressed as Eq. (14).

$$\varepsilon(k) = \delta_y(k) \qquad (14)$$

After determining surface error corresponding to individual axial disc element, the distribution over entire machined surface can be obtained by rotating the tool at specific angular

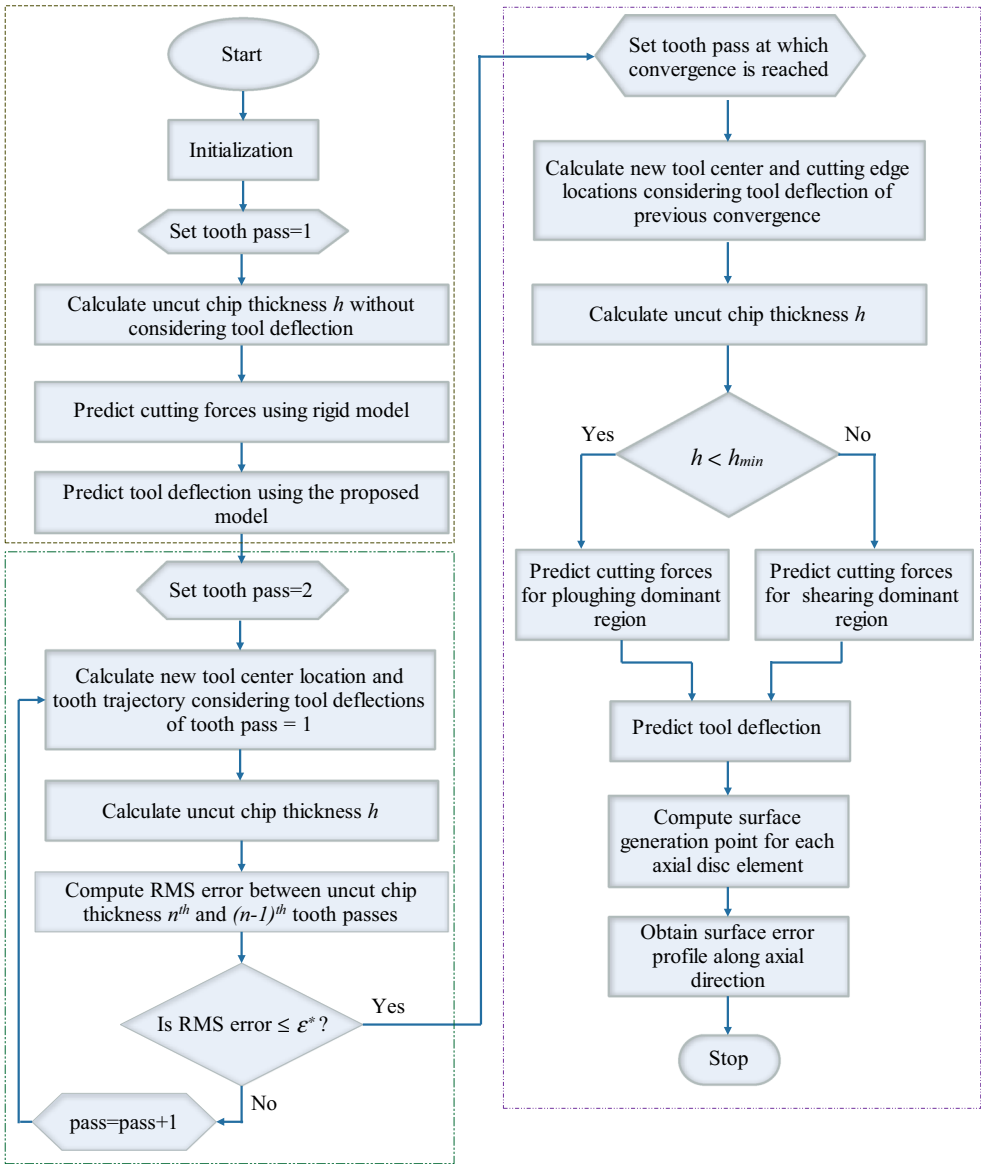


**Fig. 6** Computational algorithm to predict flexible cutting forces, tool deflections and surface error

intervals. Such procedure results into determination of 3D surface error profile in the axial and feed directions for the entire machined surface. The results of computational model are presented in the subsequent section.

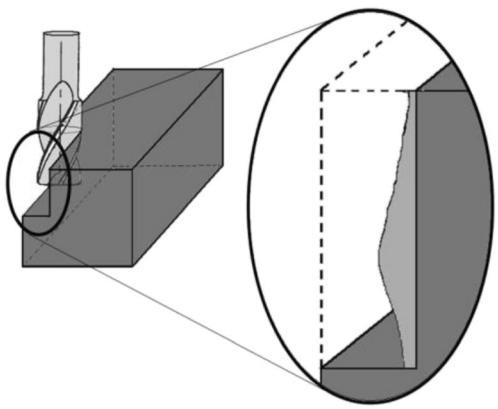

**Fig. 7** Surface error induced due to tool deflection

## 3 Results and discussion

The model outlined in previous section has been implemented in the form of computational program to estimate cutting forces and 3D surface error profile in the presence of tool deflections. The computational results are substantiated further by performing micro-milling experiments at various cutting conditions. This section discusses comparison of predicted and measured cutting forces to examine efficacy of the proposed model. In addition to cutting forces, comparison of estimated and measured 3D surface error profile is also presented in this section.

### 3.1 Comparison of predicted and measured cutting forces

To validate proposed cutting force model in the presence of tool deflections, a series of half-immersion micro-milling experiments were performed over a wide range of feed rates. These tests were conducted on a 5-Axis CNC vertical milling machine using Tungsten Carbide (WC) flat end mill of 1000 μm diameter and Aluminum 6351-T6 workpiece material. Although cutter run-out is an important parameter in the determination of process geometry parameters such as instantaneous uncut chip thickness and entry and exit angles, its magnitude was negligible for the machine used during experiments in the present study. Therefore, the effect of cutter run-out is not considered on cutting forces and tool deflections in the present study. Table 2 summarizes tool geometry, cutting conditions and other relevant parameters used during computational simulations as well as machining experiments. In order to measure and record cutting forces in *X*- and *Y*- directions, Kistler 9257BA table dynamometer and charge amplifier has been used along with data acquisition system. Figure 8 shows experimental setup and Scanning Electron Microscope (SEM) image of the tool tip.

The edge radius of the micro-end mill is determined as 2 μm approximately from the SEM image of the cutting tool while the elastic recovery rate of Aluminum work material is known to be 10% [32]. The minimum chip thickness is assumed as 30% of the edge radius for Aluminum workpiece material [32]. The present study uses relatively larger value of cutting tool overhang to have dominant effect of tool deflection-induced errors on machined surface profile. Also, relatively larger cutting tool diameter is chosen to withstand breakage of cutting tool at higher overhang length.

**Table 2** Cutting conditions used for simulation and experimental results

| Parameters | Values |
|---|---|
| Tool diameter (*d*) | 1 mm |
| Number of flute ( $N_t$) | 2 |
| Helix angle ($\theta_{hx}$) | 30° |
| Nominal rake angle ( $\alpha_n$) | 15° |
| Clearance angle ( $\gamma_n$) | 10° |
| Edge radius ( $r_e$) | 2 μm |
| Minimum chip thickness ( $h_{min}$) | $0.3r_e$ |
| Elastic recovery rate ( $p_e$) | 0.1 |
| Spindle speed (rpm) | 10,000 rpm |
| Axial depth of cut (*Adoc*) | 100 μm |
| Radial depth of cut (*Rdoc*) | 500 μm (half immersion) |
| Overhang length ($L_{oh}$) | 30 mm |
| Feed per tooth (*fpt*) | 0.2 to 10 μm/tooth |
| Tool material | Tungsten carbide (WC) |
| Workpiece material | Aluminum 6351-T6 |
| Sampling frequency | 60,000samples/s |
| Type of filter | low-pass filter |

It has been highlighted in the previous section that chip geometry is not stable during first few passes in the presence of tool deflections and it converges to a stable value after a few iterations. The model is required to incorporate this aspect while predicting cutting forces in the presence of tool deflections. The cutting forces are predicted using computational model outlined in Fig. (6), and it has been observed that the algorithm achieves convergence after few tooth passes and cutting force signal stabilizes to a normal periodic variation. The RMS deviation between instantaneous uncut chip thicknesses of two consecutive tooth passes has been computed using Eq. (12) and convergence is checked. Figure 9 shows variation of RMS deviation with tooth passes which indicates that the RMS deviation converges to a stable value after a few iterations.

Figure 10 shows comparison of predicted and experimentally measured cutting forces at three different feed rate values. These feed rate values are selected such that the effectiveness of proposed model can be examined in three different regions of micro-milling namely, shearing dominant, ploughing dominant and transition regions. Figure 10a shows comparison of predicted and experimentally measured cutting forces in a shearing dominant region. The value of feed rate is selected as 8 μm/tooth in this case which corresponds to cutting conditions identical to shearing dominant region. It can be seen that the predicted and measured cutting forces are in a good agreement with each other. It can be inferred that the proposed model predicts cutting forces accurately in the shearing dominant region where ploughing effects are insignificant. Figure 10b shows comparison of forces in ploughing dominant region where the feed rate reduces to 0.4 μm/tooth. When feed rate is lowered to such a small value, the uncut chip thickness is less than the minimum limiting value and removal of material in the form of chips does not occur. In this case, ploughing action is dominant and the mechanism of chip formation is entirely different than the shearing region. The effect of shearing action does not exist in this region and the work material flows under the cutting edge. The work material experiences elastic recovery upon flow under the edge and it rubs over flank face of the tool. This leads to significantly larger value of rubbing forces compared to the previous shearing dominant case. It can be seen that the proposed model also predicts cutting forces quite well in the ploughing dominant region. Figure 10c shows comparison of cutting forces in the transition region with corresponding feed rate of 2 μm/tooth. At this feed rate, the chip formation mechanism switches from shearing to ploughing frequently and vise-versa. This phenomenon has been termed as transition region where the model has to predict combined effect of shearing and ploughing regions while predicting cutting forces. It can be seen that the model

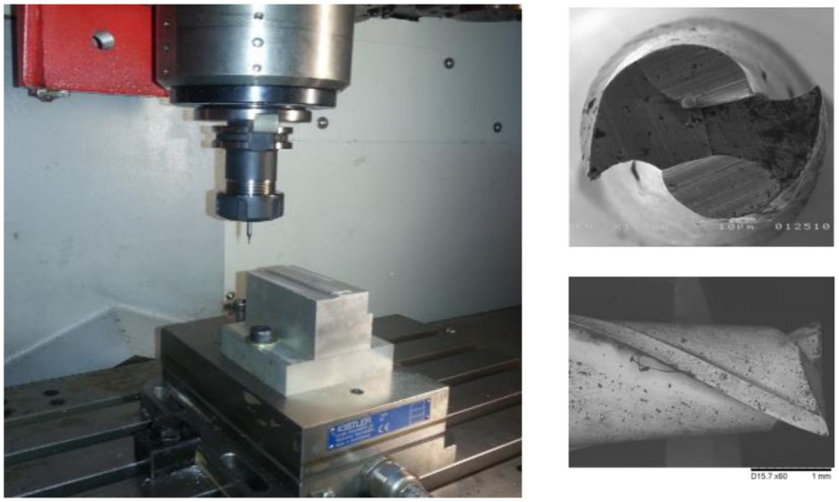

**Fig. 8** Experimental setup and SEM image of micro-end mill

predicts cutting forces quite well in transition region too. Based on comparison of predicted and measured cutting forces, it can be concluded that the proposed model estimates magnitude and profile of cutting forces in shearing, transition and ploughing regions quite accurately in the presence of tool deflections.

Furthermore, the effect of minimum chip thickness in shearing, ploughing and transition regions of chip formation process on cutting forces is well addressed in the previous work [12]. This was addressed by analyzing the root mean square (RMS) values of the cutting forces over various feed per tooth values. It was reported that the magnitude of cutting force in each of these regions is entirely different due to minimum chip thickness effect. In shearing region, cutting or shearing mechanism is dominant and RMS value of forces follow linear variation with feed rate. In a ploughing dominant region, the same trend is not followed due to significant contribution of rubbing forces generated due to elastic recovery of work material. This results into increased cutting forces although feed rates are significantly lower. In transition region, RMS of forces follow entirely different trend than shearing or ploughing dominant region due to frequent switching between these mechanisms.

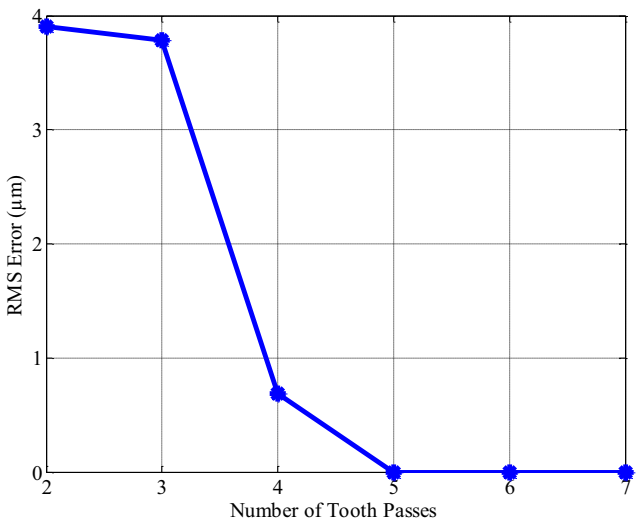


**Fig. 9** RMS deviation for convergence of uncut chip thickness computation

Figure 11a,b shows simulation results of instantaneous tool deflections versus cutter rotation angle for bottom most axial disc element at 8 and 2 μm/tooth feed rates, respectively. Once convergence is reached in the computational model, the instantaneous tool deflection values in *X*- and *Y*- direction are determined for each axial disc element using flexible cutting forces. It can be seen that the profile of instantaneous tool deflections is quite similar to cutting forces shown in Fig. 10. The instantaneous tool deflection profile also agree well with the experimentally obtained profile presented in earlier literature [38]. Based on these results, it can be concluded that the tool deflection model proposed in this paper predicts instantaneous tool deflections in micro-milling operation quite well and it can be used to determine surface error further. The subsequent section presents comparison of predicted and measured surface error profile determined using flexible cutting force and tool deflections estimated in this section.

## 3.2 Comparison of predicted and measured surface error profile

3-D surface error profile resulting due to deflections of an end mill is estimated using methodology proposed in the previous section. The methodology traces movement of individual cutting edges in the axial and feed directions and stores tool deflection value in the normal direction at the instant of surface generation. This section presents comparison of predicted and experimentally measured 3-D surface error profile to substantiate the proposed model. The present study uses

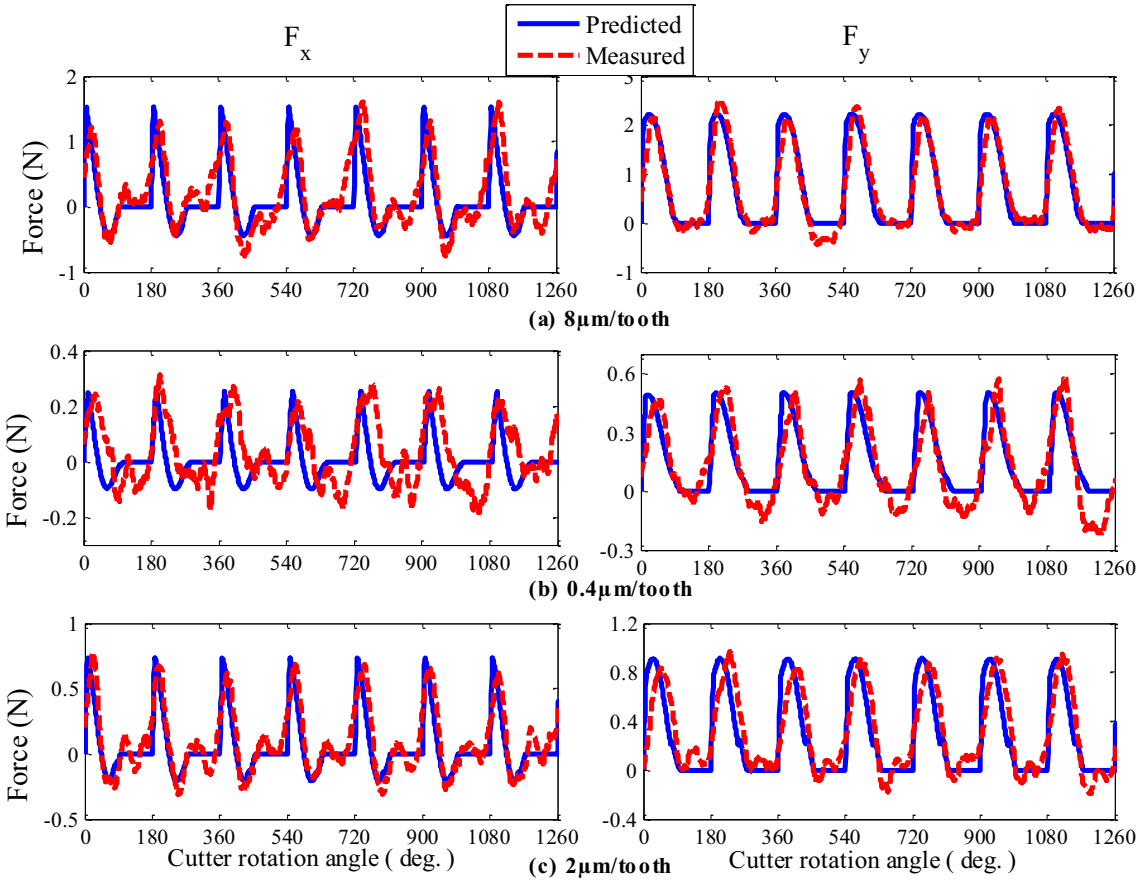


**Fig. 10** Comparison of measured and predicted forces at feed per tooth of (**a**) 8 μm/tooth, (**b**) 0.4 μm/tooth, and (**c**) 2 μm/tooth

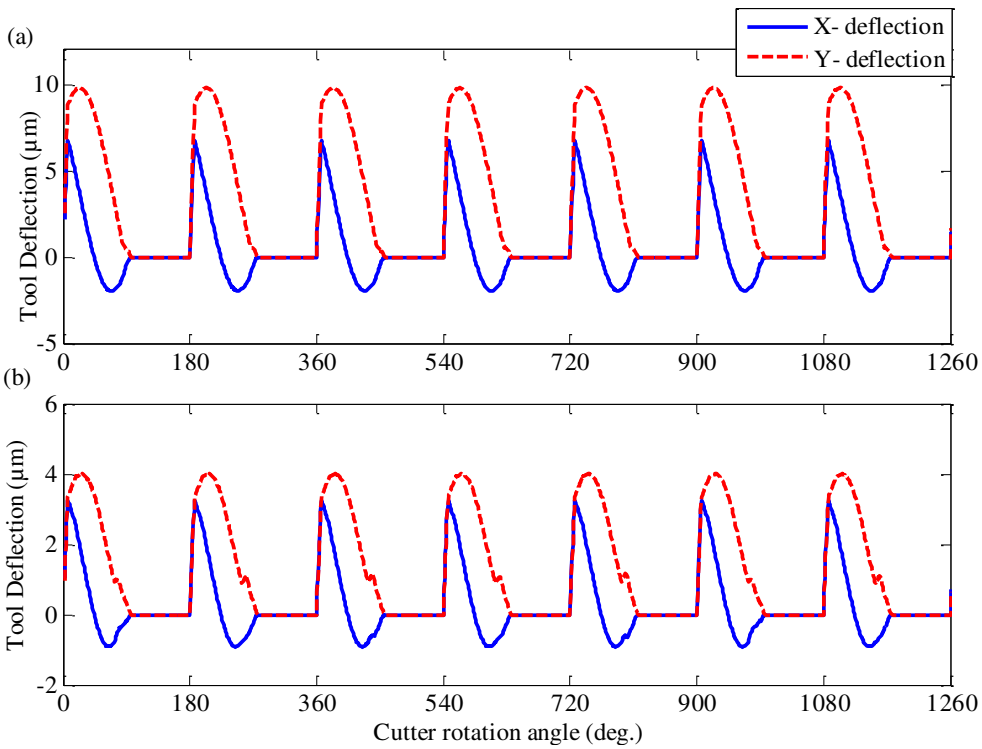


**Fig. 11** Instantaneous tool deflection at feed rate of (**a**) 8 μm/tooth and (**b**) 2 μm/tooth

MicroXAM-100 3D optical profiler to capture 3D image of machined side-wall surface.

Figure 12a shows schematic diagram of the half-immersion micro-milling process while Fig. 12b shows orientation of workpiece surface after machining to facilitate measurement of side-wall error profile using optical profiler. The optical profiler and the sample 3D image captured using the set-up are shown in Fig. 12c,d, respectively. The optical profiler focuses on the surface which includes machined side-wall as well as un-machined and blank areas. These areas can be distinctly identified in the resultant image which can be seen in Fig. 12d marked as blank space and workpiece surface (unfocused). The machined surface connected to workpiece surface (unfocused) corresponds to bottom of cut while the one connected to blank space (unfocused) represents top of the cut.

Figure 13 shows comparison of measured and predicted 3D surface error profile at different feed rate values corresponding to three machining regions. It can be seen that the 3D surface error profile estimated using proposed model follows similar trend as measured results. Based on these results, it can be inferred that the proposed methodology captures the variation of surface error quite well in all machining regions. Figure 13a shows surface error variation of machined side-wall at feed rate of 10 μm/tooth. As discussed earlier, this value of feed rate corresponds to cutting conditions identical to shearing dominant region. It can be seen that the magnitude of surface error is maximum at the bottom of cut while it is minimum at the top of cut. It can also be seen that the experimentally measured surface error profile is quite smooth indicating better surface finish. It can be attributed to cutting being shearing dominant and insignificant elastic recovery in this case. Figure 13b shows surface error variation of side-wall surface at feed rate of 0.5 μm/tooth corresponding to ploughing dominant region. The predicted profile surface error agrees well with its measured counterparts qualitatively. The experimental results indicate significant variation in the form of peaks and valleys in the machined surface implying that the generated machined surface has very high roughness value. The primary reason for increased surface roughness is elastically recovered work material which rubs over flank face of the tool and deteriorates quality of surface machined. Figure 13c shows variation of surface error variation at feed rate 2 μm/tooth corresponding to transition region. It can be seen that the predicted

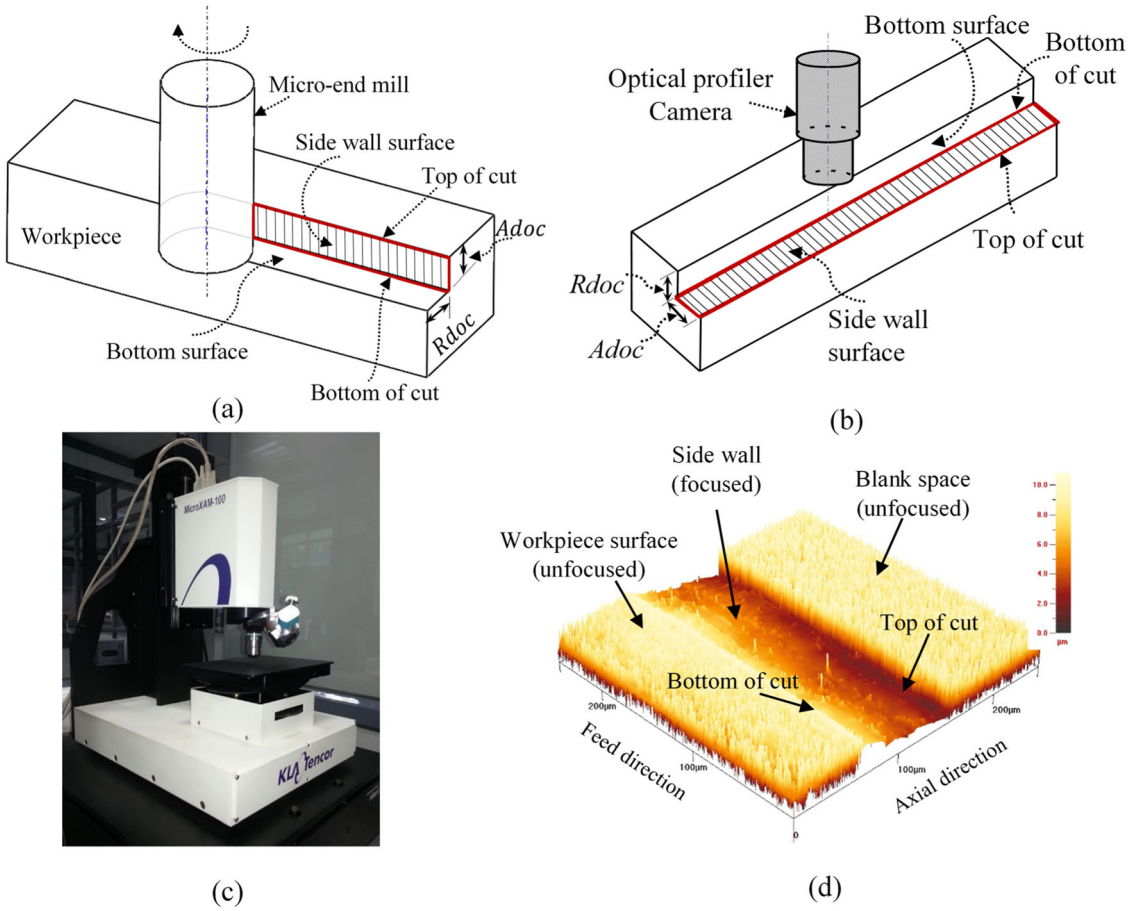


**Fig. 12** Measurement of surface error profile: (**a**) half-immersion micro-end milling operation, (**b**) schematic orientation of surface error profile measurement of machined side-wall surface, (**c**) optical Profiler, and (**d**) captured 3D image

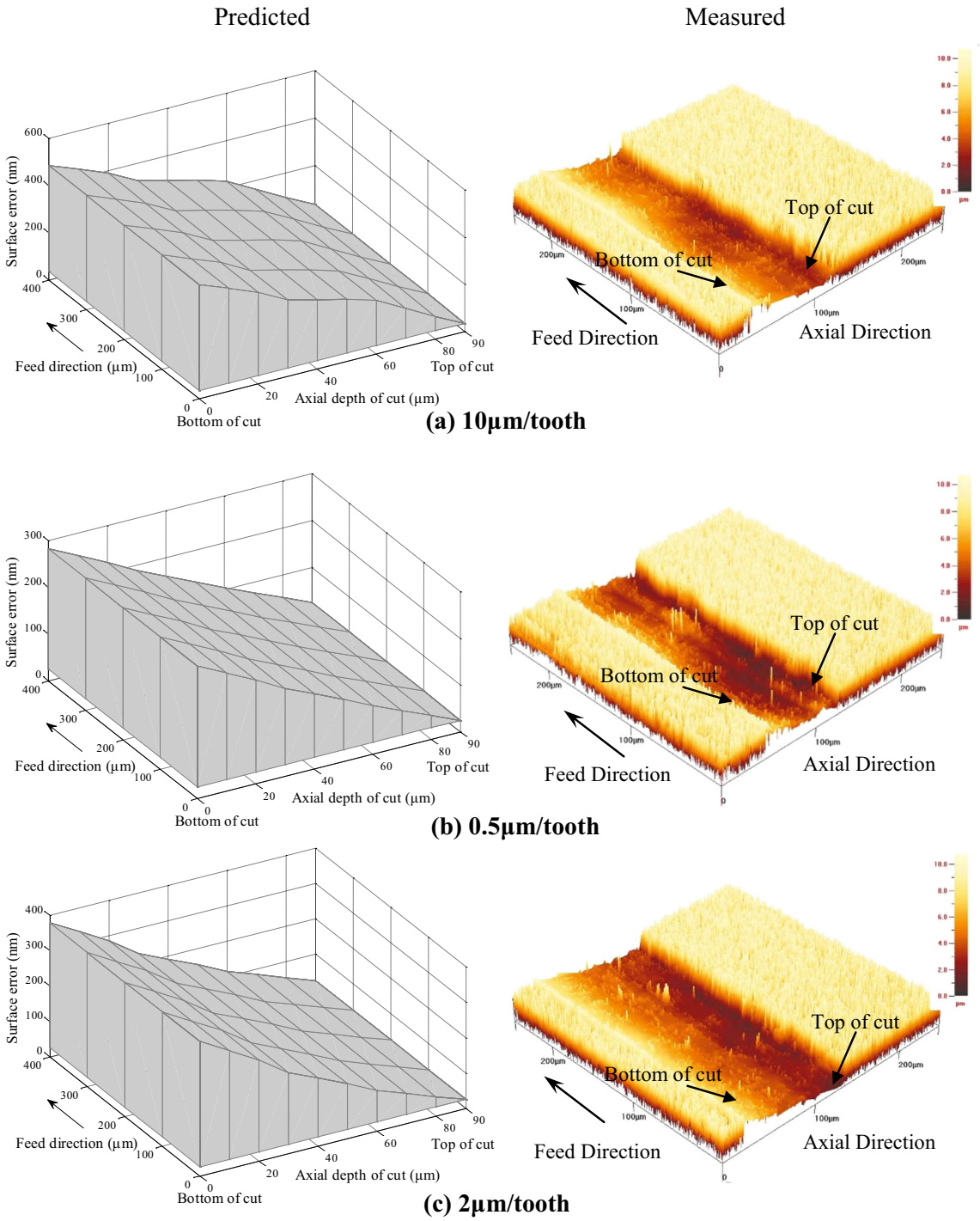


**Fig. 13** Comparison of measured and predicted 3D surface error profile. (**a**) 10 µm/tooth. (**b**) 0.5 µm/tooth. (**c**) 2 µm/tooth

surface error profile agree well qualitatively with experimentally measured results. It can be seen that the quality of surface finish in transition region is relatively better compared to ploughing region in Fig. 13b but poorer than shearing region in Fig. 13a. This is due to frequent switching of chip formation mechanism from shearing to ploughing region and vice-versa. From the results presented in this section, it can be concluded that the proposed methodology can predict cutting forces and tool deflection-induced surface error profile in all three zones of micro-milling operation. Although tool deflections play significant role in prediction accuracy of cutting forces and surface error, dynamic vibrations of the tool tip of influences accuracy of the model substantially. The surface roughness is comparable to surface error in ploughing and transition regions. Incorporating these factors in proposed computational model will improve the prediction accuracy of the model and

enable quantitative validation of the surface error, which can be further work of study.

## 4 Conclusions

The paper presented a methodology to predict cutting force, tool deflection and surface error by developing a flexible force model which considers the effect of tool deflection on cutting forces in micro-milling. As tool deflection alters tooth trajectories and instantaneous uncut chip thickness, the rigid cutting force model is modified suitably to consider the effect of deflections. An iterative scheme is presented to predict cutting forces in the presence of tool deflections. The cutting force model incorporates the effects of tool deflections on cutting forces along with the important process characteristics of micro-milling. A tool deflection model which partitions an end mill into three different regions namely shank, taper and a fluted portion is presented in the study. A moment-area method has been used to estimate deflections of the shank and taper parts whereas deflection of the fluted area is computed considering cutting tool as a cantilever beam with non-uniform forces acting along the contact area. It is realized that the deflection of an end mill causes significant deviation of the tool center location resulting into change of tooth trajectories and uncut chip geometry. To incorporate these effects, an iterative methodology is proposed to predict cutting forces. The RMS deviation between average chip thicknesses of successive iterations is used as a measure to achieve the convergence of the algorithm. It is observed that the chip thickness converges to a stable value after a few iterations and the values of cutting force and tool deflection determined at convergence point can be further used in estimating surface error. It is observed that the variation of instantaneous tool deflection with cutter rotation angle predicted using proposed methodology agree well with measured cutting force profile and previous results reported in the literature. The surface error variation in axial and feed direction is computed using cutting forces and tool deflection values determined from iterative algorithm using surface generation mechanism. The proposed models are implemented in the form of a computational program to predict cutting forces and surface error profile in the presence of tool deflection over wide range of feed rates. The estimated results are also corroborated by conducting micro-milling tests and measurement of surface error using 3-D optical microscope. It is observed that the proposed model predicts magnitude and profile of cutting forces quite well for all cutting cases of micro-milling. From qualitative validation of surface error model, it is observed that the predicted surface error profile follows the same profile as experimentally captured 3D image of the machined side-wall surface. In order to further improve the prediction accuracy of the proposed computational model, considering the dynamic vibration of the tip of the tool and surface roughness is important and that can be further research work. Based on outcomes of the paper, it has been realized that tool deflection has significant effect on the accuracy of machined components. The proposed model can be useful for process planner in selecting optimum cutting parameters that controls cutting forces and associated tool deflections which results into improved machining tolerances with enhanced productivity.

**Acknowledgements** The authors thank Dr. J RamKumar, Mechanical Engineering Department at the IIT Kanpur for his permission to use the laboratory facilities to conduct micro-milling experiments and staff of the Nanoscale Research Facility (NRF) at the IIT Delhi for useful support during measurement of surface error variation.

**Nomenclature** $r$, Radius of a cutting tool (mm); $N_t$, Number of teeth; $\alpha_e$, $\gamma_e$, Effective rake and clearance angle (°); $\varphi_p$ , Pitch angle of the cutting tool (°); $r_e$, Edge radius (mm); $\theta_{hx}$ , Helix angle of the cutting tool (°); $fpt$, Feed per tooth (mm/tooth); $h$, Instantaneous chip thickness (mm); $h_{min}$, Minimum chip thickness (mm); $h_{er}$, Elastic recovery height (mm); $p_e$, Elastic recovery rate of workpiece material; $dz$ , Thickness of an axial disc element (mm); $\Delta h_s$, Thickness of element of uncut chip area (mm); $\Delta h_p$, $\Delta h_{er}$ , Thickness of element of ploughed material and elastically recovered material (mm); $dA_a$, $dA_b$, $dA_c$, Area of uncut chip element, elemental ploughed area, and area of elastically recovered element ($mm^2$); $dF_{ns}$, $dF_{fs}$, Normal and frictional components of shearing force (N); $dF_{np}$, $dF_{fp}$, Normal and frictional components of ploughing force (N); $dF_{nr}$, $dF_{fr}$, Normal and frictional components of rubbing force (N); $dF_{rs}$, $dF_{ts}$, Shearing forces in radial and tangential directions (N); $dF_{rp}$, $dF_{tp}$, Ploughing forces in radial and tangential directions (N); $dF_x$, $dF_y$, $X$ and $Y$ components of elemental force (N); $K_{re}$, $K_{te}$ , Edge coefficients in radial and tangential directions (N/mm); $K_{ns}$, $K_{fs}$ , Shearing coefficients in normal and frictional directions ($N/mm^2$); $K_{np}$, $K_{fp}$, Ploughing coefficients in normal and frictional directions ($N/mm^2$); $K_{nr}$, $K_{fr}$, Rubbing coefficients in normal and frictional directions ($N/mm^2$); $i$, $j$, $k$, Indices for tooth, angular rotation and axial disc element; $u$, $v$, $w$, Indices for elemental uncut chip area, ploughed material, and elastically recovered material; $\beta$, Angular position of a cutting edge at $i$, $j$, $k$ (°); $\theta$, Cutter rotation angle for the cutting point on bottom most axial disc element (°); $L_{oh}$ , Over hang length from tool holder to the free end of a tool; $E$, Young's Modulus of a cutting tool material ($N/mm^2$); $L_f$, $L_s$, $L_t$, Length of flute, shank and taper parts (mm); $I_f$, $I_s$, $I_t$ , Area moment of inertia of flute, shank and taper parts ($mm^4$); $h_n(\theta)$, $h_{n-1}(\theta)$, Uncut chip thickness to be removed by tooth pass $n$ and $n-1$ at each engaged angle of rotation ($\theta$); $\delta_x$, $\delta_y$, Tool deflections in $X$- and $Y$- directions; $\varepsilon(k)$, Surface error at $k$th axial disc element



## References

1. Altinga L, Kimurab F, Hansena HN, Bissacco GB (2003) Micro engineering. CIRP Ann Manuf Technol 52:635–657
2. Chae J, Park SS, Freiheit T (2006) Investigation of micro-cutting operations. Int J Mach Tools Manuf 46:313–332. https://doi.org/10.1016/j.ijmachtools.2005.05.015
3. Bao WY, Tansel IN (2000) Modeling micro-end-milling operations. Part I: analytical cutting force model. Int J Mach Tools Manuf 40: 2155–2173. https://doi.org/10.1016/S0890-6955(00)00054-7

4. Cheng KAI, Huo D (2013) Micro-cutting: fundamentals and applications. Wiley, UK
5. Weule H, Huntrupl V, Tritschlerl H (2001) Micro-cutting of steel to meet new requirements in miniaturization. CIRP Ann Manuf Technol 50:61–64
6. Kim JD, Kim DS (1995) Theoretical analysis of micro-cutting characteristics in ultra-precision machining. 49:387–398
7. Vogler MP, Kapoor SG, DeVor RE (2004) On the modeling and analysis of machining performance in micro-endmilling, part II: cutting force prediction. J Manuf Sci Eng 126:695. https://doi.org/10.1115/1.1813471
8. Park SS, Malekian M (2009) Mechanistic modeling and accurate measurement of micro end milling forces. CIRP Ann Manuf Technol 58:49–52. https://doi.org/10.1016/j.cirp.2009.03.060
9. Liu X, DeVor RE, Kapoor SG, Ehmann KF (2004) The mechanics of machining at the microscale: assessment of the current state of the science. J Manuf Sci Eng 126:666. https://doi.org/10.1115/1.1813469
10. Moges TM, Desai KA, Rao PVM (2016) Improved process geometry model with cutter runout and elastic recovery in micro-end milling. Proc of 44th NAMRI/SME 5:478–494. https://doi.org/10.1016/j.promfg.2016.08.040
11. Bissacco G, Hansen HN, Slunsky J (2008) Modelling the cutting edge radius size effect for force prediction in micro milling. CIRP Ann Manuf Technol 57:113–116. https://doi.org/10.1016/j.cirp.2008.03.085
12. Moges TM, Desai KA, Rao PVM (2017) On modeling of cutting forces in micro-end milling operation. Mach Sci Technol 344:1–20. https://doi.org/10.1080/10910344.2017.1336179
13. Vogler MP, DeVor RE, Kapoor SG (2004) On the modeling and analysis of machining performance in micro-endmilling, part I: surface generation. J Manuf Sci Eng 126:685. https://doi.org/10.1115/1.1813470
14. Kouravand S, Imani BM (2014) Developing a surface roughness model for end-milling of micro-channel. Mach Sci Technol 18:299–321. https://doi.org/10.1080/10910344.2014.897846
15. Lee K, Dornfeld D (2005) Micro-burr formation and minimization through process control. Precis Eng 29:246–252. https://doi.org/10.1016/j.precisioneng.2004.09.002
16. Kiswanto G, Zariatin DL, Ko TJ (2015) The effect of spindle speed, feed-rate and machining time to the surface roughness and burr formation of aluminum alloy 1100 in micro-milling operation. J Manuf Process 16:435–450. https://doi.org/10.1016/j.jmapro.2014.05.003
17. Wang Z, Kovvuri V, Araujo A et al (2016) Built-up-edge effects on surface deterioration in micromilling processes. J Manuf Process 24:321–327. https://doi.org/10.1016/j.jmapro.2016.03.016
18. Dow TA, Miller EL, Garrard K (2004) Tool force and deflection compensation for small milling tools. Precis Eng 28:31–45. https://doi.org/10.1016/S0141-6359(03)00072-2
19. Uriarte L, Herrero A, Zatarain M et al (2007) Error budget and stiffness chain assessment in a micromilling machine equipped with tools less than 0.3mm in diameter. Precis Eng 31:1–12. https://doi.org/10.1016/j.precisioneng.2005.11.010
20. Biermann D, Kahnis P (2009) Analysis and simulation of size effects in micromilling. Prod Eng 4:25–34. https://doi.org/10.1007/s11740-009-0201-1
21. Bao WY, Tansel IN (2000) Modeling micro-end-milling operations. Part II: tool run-out. Int J Mach Tools Manuf 40:2175–2192. https://doi.org/10.1016/S0890-6955(00)00055-9
22. Zaman MT, Kumar AS, Rahman M, Sreeram S (2006) A three-dimensional analytical cutting force model for micro end milling operation. Int J Mach Tools Manuf 46:353–366. https://doi.org/10.1016/j.ijmachtools.2005.05.021
23. Kang IS, Kim JS, Kim JH et al (2007) A mechanistic model of cutting force in the micro end milling process. J Mater Process Technol 187–188:250–255. https://doi.org/10.1016/j.jmatprotec.2006.11.155
24. Jun MBG, Liu X, DeVor RE, Kapoor SG (2006) Investigation of the dynamics of microend milling—part I: model development. J Manuf Sci Eng 128:893. https://doi.org/10.1115/1.2193546
25. Altintas Y, Jin X (2011) Mechanics of micro-milling with round edge tools. CIRP Ann Manuf Technol 60:77–80. https://doi.org/10.1016/j.cirp.2011.03.084
26. Rao S, Shunmugam MS (2012) Analytical modeling of micro end-milling forces with edge radius and material strengthening effects. Mach Sci Technol 16:205–227. https://doi.org/10.1080/10910344.2012.673966
27. Lai X, Li H, Li C, et al (2008) Modelling and analysis of micro scale milling considering size effect, micro cutter edge radius and minimum chip thickness. Int J Mach Tools Manuf 48:1–14. doi: https://doi.org/10.1016/j.ijmachtools.2007.08.011
28. Afazov SM, Ratchev SM, Segal J (2010) Modelling and simulation of micro-milling cutting forces. J Mater Process Technol 210:2154–2162. https://doi.org/10.1016/j.jmatprotec.2010.07.033
29. Jin X, Altintas Y (2012) Prediction of micro-milling forces with finite element method. J Mater Process Technol 212:542–552. https://doi.org/10.1016/j.jmatprotec.2011.05.020
30. Li C, Lai X, Li H, Ni J (2007) Modeling of three-dimensional cutting forces in micro-end-milling. J Micromech Microeng 17:671–678. https://doi.org/10.1088/0960-1317/17/4/001
31. Pérez H, Vizán A, Hernandez JC, Guzmán M (2007) Estimation of cutting forces in micromilling through the determination of specific cutting pressures. J Mater Process Technol 190:18–22. https://doi.org/10.1016/j.jmatprotec.2007.03.118
32. Malekian M, Park SS, Jun MBG (2009) Modeling of dynamic micro-milling cutting forces. Int J Mach Tools Manuf 49:586–598. https://doi.org/10.1016/j.ijmachtools.2009.02.006
33. Jun MBG, Goo C, Malekian M, Park S (2012) A new mechanistic approach for micro end milling force modeling. J Manuf Sci Eng 134:11006. https://doi.org/10.1115/1.4005429
34. Kline WA, DeVor RE, Lindberg JR (1982) The prediction of cutting forces in end milling with application to cornering cut. Int J Mach Tool Des Res 22:7–22
35. Ryu SH, Lee HS, Chu CN (2003) The form error prediction in side wall machining considering tool deflection. Int J Mach Tools Manuf 43:1405–1411. https://doi.org/10.1016/S0890-6955(03)00183-4
36. Mijušković G, Krajnik P, Kopač J (2013) Analysis of tool deflection in micro milling of graphite electrodes. Int J Adv Manuf Technol 76:209–217. https://doi.org/10.1007/s00170-013-5536-2
37. Budak E, Altintas Y (1995) Modeling and avoidance of static form errors in peripheral milling of plates. Int J Mach Tools Manuf 35:459–476
38. Mamedov A, Layegh KSE, Lazoglu I (2015) Instantaneous tool deflection model for micro milling. Int J Adv Manuf Technol 79:769–777. https://doi.org/10.1007/s00170-015-6877-9
39. Tsai J, Liao C (1999) Finite-element modeling of static surface errors in the peripheral milling of thin-walled workpieces. 94:235–246
40. Gye H-R, Song B-U, Lim Y-S, et al (2013) Prediction of cutting force and tool deflection in micro flat end milling. Int J Mater Mech Manuf 1:13–16. doi: https://doi.org/10.7763/IJMMM.2013.V1.3
41. Uriarte L, Azcárate S, Herrero A, et al (2008) Mechanistic modelling of the micro end milling operation. Proc Inst Mech Eng Part B J Eng Manuf 222:23–33. doi: https://doi.org/10.1243/09544054JEM837
42. Rodríguez P, Labarga JE (2013) A new model for the prediction of cutting forces in micro-end-milling operations. J Mater Process Technol 213:261–268

43. Zhang X, Ehmann KF, Yu T, Wang W (2016) Cutting forces in micro-end-milling processes. Int J Mach Tools Manuf 107:21–40. https://doi.org/10.1016/j.ijmachtools.2016.04.012
44. Mamedov A, Layegh KSE, Lazoglu I (2013) Machining forces and tool deflections in micro milling. Procedia CIRP 8:147–151. https://doi.org/10.1016/j.procir.2013.06.080
45. Wang S, Chen D, Jang M, Tsooj S (2012) Development of micro milling force model and cutting parameter optimization. Trans Nonferrous Met Soc China 22:s851–s858. https://doi.org/10.1016/S1003-6326(12)61815-9
46. Kops L, Vo DT (1990) Determination of the equivalent diameter of an end mill based on its compliance. 3:93–96
47. Hibbeler RC (2014) Mechanics of materials. In: Deflection of beams and shafts, 9th edn. Prentice Hall, USA, pp 573–659
48. Sutherland JW, Devor RE (2016) An improved method for cutting force and surface error prediction in flexible end milling systems. J Manuf Sci Eng 1986;108:269–279
49. Wan M, Zhang WH (2005) Calculations of chip thickness and cutting forces in flexible end milling. Int J Adv Manuf Technol 29:637–647. https://doi.org/10.1007/s00170-005-2572-6
50. Desai KA, Rao PVM (2012) On cutter deflection surface errors in peripheral milling. J Mater Process Technol 212:2443–2454. https://doi.org/10.1016/j.jmatprotec.2012.07.003